AGU PUBLICATIONS

Geophysical Research Letters

RESEARCH LETTER
10.1002/2015GL065975

Key Points:
- Seismic velocity variations were examined with seismic noise correlations in a mine during a blast
- A sudden decrease, gradual relaxation, and permanent changes in the seismic velocity are observed
- Elastic modelling shows that the permanent changes in velocity are due to changes in static stress

Supporting Information:
- Text S1 and Figure S1

Correspondence to:
G. Olivier,
gjf.olivier@gmail.com

Citation:
Olivier, G., F. Brenguier, M. Campillo, P. Roux, N. M. Shapiro, and R. Lynch (2015), Investigation of coseismic and postseismic processes using in situ measurements of seismic velocity variations in an underground mine, *Geophys. Res. Lett.*, *42*, doi:10.1002/2015GL065975.

Received 18 SEP 2015
Accepted 25 OCT 2015
Accepted article online 4 NOV 2015

Investigation of coseismic and postseismic processes using in situ measurements of seismic velocity variations in an underground mine

G. Olivier[1,2], F. Brenguier[1], M. Campillo[1], P. Roux[1], N. M. Shapiro[3], and R. Lynch[2]

[1]Institut des Sciences de la Terre, Université Joseph Fourier, Grenoble, France, [2]Institute of Mine Seismology, Kingston, Tasmania, Australia, [3]Institut de Physique du Globe de Paris, Paris, France

Abstract The in situ mechanical response of a rock mass to a sudden dynamic and static stress change is still poorly known. To tackle this question, we conducted an experiment in an underground mine to examine (1) the influence of dynamic and static stress perturbations on seismic velocities, (2) elastic static stress changes, and (3) induced earthquake activity associated with the blast and removal of a portion of hard rock. We accurately (0.01%) measured seismic velocity variations with ambient seismic noise correlations, located aftershock activity, and performed elastic static stress modeling. Overall, we observe that the blast induced a sudden decrease in seismic velocities over the entire studied area, which we interpreted as the damage due to the passing of strong seismic waves. This sudden process is followed by a slow relaxation lasting up to 5 days, while seismic activity returns to its background level after 2 days. In some locations, after the short-term effects of the blast have subsided, the seismic velocities converge to new baseline levels and permanent changes in seismic velocity become visible. After comparing the spatial pattern of permanent seismic velocity changes with elastic static stress modeling, we infer that the permanent seismic velocity changes are due to the change in the static volumetric stress induced by the removal of a solid portion of rock by the blast. To our knowledge, this is the first observation of noise-based permanent seismic velocity changes associated with static stress changes.

1. Introduction

The behavior of the crust shortly after earthquakes has been the subject of numerous studies, but many coseismic and postseismic processes remain poorly understood. These processes are important to properly model and understand the behavior of faults and earthquake cycles. Damage and healing of the bulk rock mass, postseismic deformation, and the mechanisms of triggering are still not well understood [*Scholz*, 2002; *Gonzalez-Huizar and Velasco*, 2011; *Johnson et al.*, 2015]. This is partly due to the complexity of the stress distribution and heterogeneities in the fault zone and partly due to the lack of information and measurements close to faults. Laboratory stick slip experiments have provided insights into earthquake cycles and dynamic triggering [*Johnson and Jia*, 2005], but real faults have complex frictional properties and can be triggered by environmental factors like groundwater depletion [*Amos et al.*, 2014], fluid pressure [*Shapiro et al.*, 2003], dynamic stress perturbations from large earthquakes [*Gomberg et al.*, 2001; *Hill et al.*, 1993; *Gomberg et al.*, 2004], and quasi-static stress changes from slow-slip events [*Bouchon et al.*, 2011], which makes dynamic triggering and real earthquakes hard to model [*Bakun and Lindh*, 1985].

The mechanism of dynamic triggering is not well understood since the dynamic strain from large earthquakes is small beyond a few fault radii [*Gomberg et al.*, 2003]. Often, delay times of minutes to hours between the initial large event and the "triggered" microseismic events are reported, which makes it hard to attribute the triggering of the latter to the former. Earthquakes can be considered to be dynamically triggered if the start time is within seconds of the arrival of the direct waves of the triggering event, allowing for a reasonable nucleation time [*Tape et al.*, 2013]. In other cases, the occurrence of triggered events is attributed to changes in the elastic static stress induced by the large earthquakes, where the relatively small change in elastic stress by a large earthquake moves another fault closer to failure [*Stein*, 1999; *Mantovani et al.*, 2010]. This mechanism allows for much larger delay times between the initial earthquake and triggered earthquakes.

To better understand how the crust responds to large earthquakes, there is a need to improve current methods for measuring in situ stress change and damage near active faults. Strain cells, tiltmeters, and extensometers have all been used in active fault zones, but the measurements are very localized and do not provide a complete picture of what is happening at depth.

On the other hand, seismic velocities of rock are sensitive to changes in applied stress [*Nur*, 1971; *O'Connell and Budiansky*, 1974; *Lockner et al.*, 1977]. The relation between applied stress and seismic velocity has been attributed to the opening and closing of microcracks, which will decrease and increase the seismic velocities, respectively. If the seismic velocity variations can be determined to the required accuracy, known stress changes like the deformation of the Earth's crust due to the earth tides or the stress caused by atmospheric air pressure changes can be used to calibrate these stress-induced velocity variations [*Fazio et al.*, 1973; *Reasonberg and Aki*, 1974; *Leary et al.*, 1979]. Unfortunately, the sensitivity of seismic velocity to applied stress is low [*Yamamura et al.*, 2003], so that the seismic velocities have to be measured very accurately to be able to detect the processes of interest.

Over the last decade, seismic noise correlations have emerged as a method that provides sufficient resolution to resolve small variations (below 0.1%) in seismic velocity [*Sens-Schönfelder and Wegler*, 2006]. Cross-correlating ambient seismic noise can be used to construct estimates of the seismic Green's function between sensor pairs, effectively turning one of the sensors into a virtual source [*Shapiro and Campillo*, 2004; *Roux and Kuperman*, 2004; *Sabra et al.*, 2005; *Campillo*, 2006]. With this method it has been shown that large earthquakes have measurable effects on seismic velocity [*Brenguier et al.*, 2008a; *Cheng et al.*, 2010]. These studies reported significant coseismic velocity drops along with a gradual relaxation back to preseismic levels. The velocity drops have been shown to be located in the rupture zone of the large event or in areas where the susceptibility of seismic velocities to stress change is large, like volcanic regions with high pore pressure [*Brenguier et al.*, 2014]. Significant precursory velocity changes have also been reported for volcanic eruptions [*Brenguier et al.*, 2008b], mud landslides [*Mainsant et al.*, 2012], and even earthquakes [*Niu et al.*, 2008].

In this study, we investigate whether accurate measurements of seismic velocity variations using noise correlation methods can provide insights into the immediate and long-term effects of a sudden dynamic stress perturbation on the surrounding rock. The experiment was conducted in an environment that is well instrumented and fits naturally between laboratory and crustal scale—an active underground mine.

2. Data and Methods

In an effort to understand the immediate and long-term effects of a sudden dynamic stress perturbation and elastic static stress changes on the surrounding medium, we conducted a small-scale experiment in an active underground mine while recording continuous seismic data with the standard mine Institute of Mine Seismology (IMS) microseismic monitoring network. The seismic network consists of 18 short-period geophones. The experiment entailed the simultaneous detonation of multiple explosives in a 20 m^3 volume in a mining tunnel and examining the effects on the surrounding rock by considering triggered seismicity, seismic velocity variations, and modeled elastic static stress behavior. The blast produced peak ground motions of up to 30 mm/s on geophones roughly 50 m away.

The location of the blast and subsequent aftershocks relative to the mining tunnels and sensors are shown in Figure 1. The aftershocks are not grouped evenly around the location of the blast but appear clustered. The locations of the aftershocks stay reasonably constant over a 2 day period, and no systematic migration patterns were observed. The time distribution of the aftershocks follows Omori's law with a p value of 0.48, which seems low but is reasonable in a mine setting [*Vallejos and McKinnon*, 2010].

To better understand the immediate effect of the blast on the surrounding medium and the mechanism behind the aftershocks, we examined hourly measurements of the seismic velocity variations. Most of the previous studies where ambient seismic noise correlations have been used to measure seismic velocity variations have used surface seismic sensor arrays. In these scenarios, the surface waves from the interaction of the ocean waves with the solid earth provide stable seismic noise sources that can be used to make daily measurements of seismic velocity variations. However, the wavelengths of these surface waves are too large to provide sufficient sensitivity and resolution for many small-scale industrial environments (like mines).

Recently, it has been shown that the noise generated by mining activity can be used to construct good estimates of the seismic Green's function if the noise is carefully selected [*Olivier et al.*, 2015]. The processing

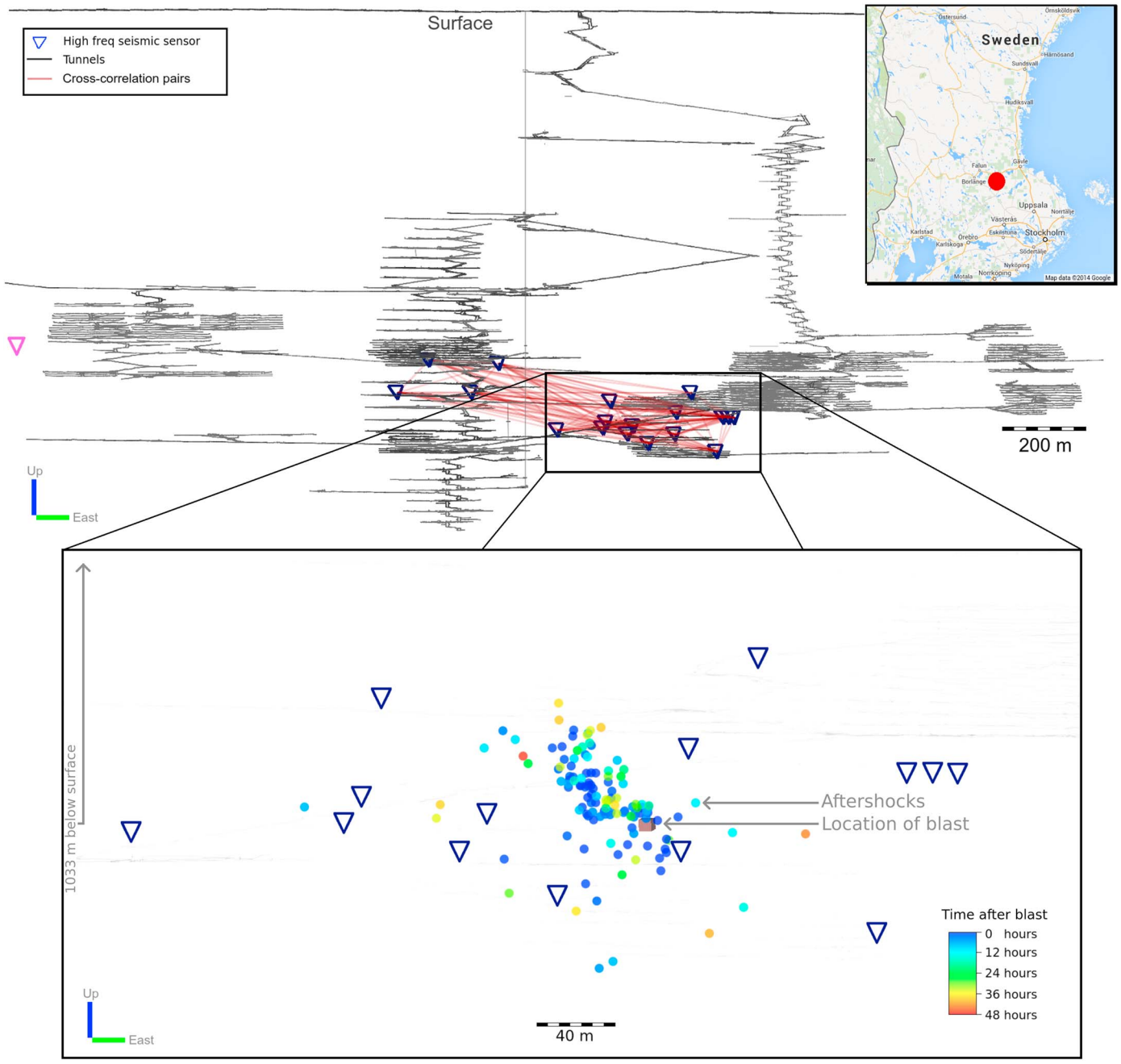

Figure 1. (top) Side view of the mine plans of Boliden's Garpenberg mine in Sweden along with the locations of the seismic sensors. (bottom) Zoomed view of the location of the blast and the proceeding aftershocks. The aftershocks are colored by the amount of time elapsed after the blast. The aftershocks are not located homogeneously around the area where blasting occurred, and no clear migration pattern is visible.

scheme that we employed in this study is a variation of the method described in detail in *Olivier et al.* [2015] and only briefly outlined here. Every hour of continuous data is split into 10 s sections, spectrally whitened between 20 and 240 Hz and one-bit normalized. The resulting sections are cross correlated among station pairs. If the 10 s cross-correlation function (CCF) for a specific station pair has a signal-to-noise ratio of 2 or more in a window around the lag time corresponding to the expected arrival time of the primary *S* wave, the CCF is added to the hour stack for this station pair. The resulting stack is used as the hourly CCF.

This processing scheme succeeds in recovering stable estimates of the seismic Green's function every hour. All CCFs for one station pair are shown in Figure 2. Each colored line in the bottom part represents an hourly CCF, while the average for the entire time period is shown at the top of the figure. A remarkable feature visible

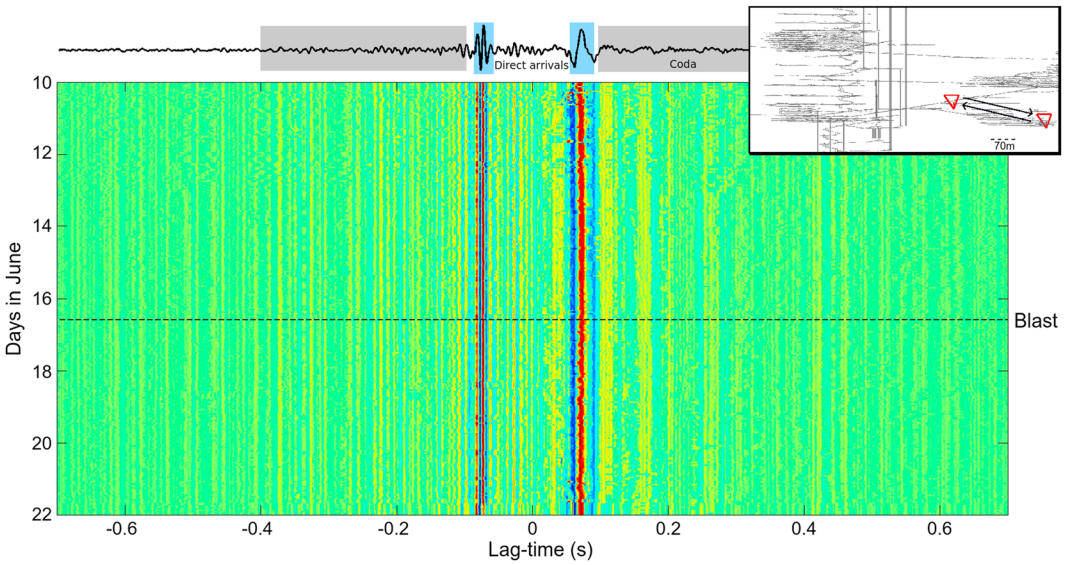

Figure 2. Stack of (top) all cross-correlation functions and (bottom) hourly cross-correlation functions for one station pair for the 12 day period. The time of the blast is indicated by a black dotted line. The cross-correlation functions appear stable for up to at least 0.7 s lag time. The inset indicates which stations were used to construct the cross-correlation functions. The grey rectangles indicate the windows that were considered when measuring the velocity variations (after the direct *S* wave, up to 0.4 s).

here is the temporal stability of the cross-correlation functions, especially in the coda of the CCFs. The coda of the CCFs is expected to be more stable as a function of time than the direct arrivals. This is due to the fact that the direct arrivals are more sensitive to changes in seismic sources than the coda when constructing CCFs [*Froment et al.*, 2010].

These stable hourly estimates of the seismic Green's function are used to measure time-dependent relative seismic velocity variations by using the moving window cross-spectral technique [*Poupinet et al.*, 1984; *Clarke et al.*, 2011]. To reduce the potential errors due to changes in the seismic sources, this method is only used to measure changes of the seismic velocity in the coda of the CCFs. Relative velocity variations were measured in the frequency band 100–240 Hz and in the lag time window between 0.02 s after the expected arrival of the direct *S* wave and up to 0.4 s. A large number of different processing parameters were tested, and these particular parameters resulted in the smallest average misfits in the linear regression measurements. The stable reconstructions of the seismic Green's functions along with the MWCS technique enabled us to resolve velocity variations as small as 0.01%.

In order to obtain the time-dependent velocity variations for an entire period, it is common to measure changes between individual CCFs and an arbitrary reference CCF. The reference CCF can be the average of all available CCFs or the average of a subset. In an environment where it is possible that the CCFs can change due to medium or source changes, the use of this method could introduce large errors if the CCFs become incoherent over time [*Hillers et al.*, 2014].

Recently, a new way to determine the time-dependent seismic velocity variations has been proposed that eliminates the need to introduce an arbitrary reference function. In this method, the travel time variation between each CCF and all the other CCFs is measured and a Bayesian least squares inversion is performed to find the time-dependent seismic velocity variations [*Brenguier et al.*, 2014]. This method requires $\frac{K\times(K-1)}{2}$ measurements compared to K measurements when using an arbitrary reference. However, the advantage of this method is that all measurements, weighted by their coherences, are inverted simultaneously, which reduces the potential errors introduced by a changing CCF.

In order to locate the regions where the velocity variations occur, we average the velocity variations for the $N-1$ cross-correlation pairs involving a specific sensor (where N is the number of sensors). In the frequency band where velocity variations are measured, the seismic wavefield is diffuse due to the scattering caused by the mining excavations and tunnels [*Olivier et al.*, 2015]. As a result the sensitivity kernels, based on diffusion approximations, have a pronounced maximum close to the sensors. The average of $N-1$ velocity variations

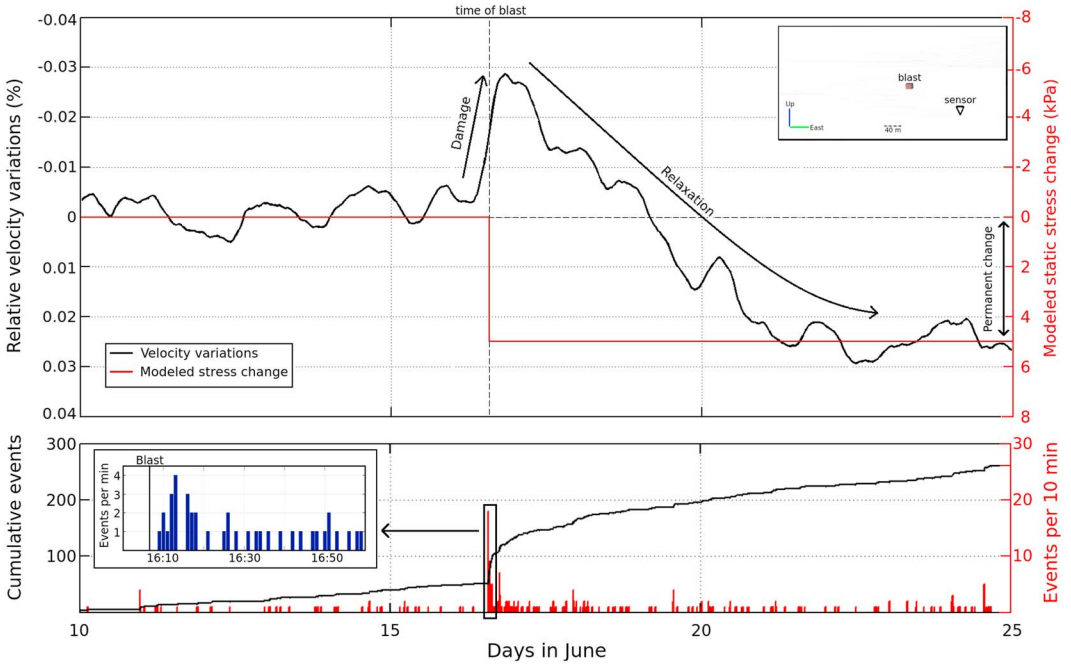

Figure 3. (top) Seismic velocity variations averaged for one sensor. Three features are present: an immediate decrease during the blast, relaxation that takes up to 5 days after the blast, and the permanent change in baseline of the seismic velocity. (bottom) The cumulative number of events recorded during the 15 day period, along with the number of events recorded every 10 min. The inset shows a zoomed view of the hour in which the blasting took place. The seismic activity rate peaks at 7 min after the blast.

involving a specific sensor is therefore a good approximation for the velocity change at this sensor. This averaging process also decreases the errors in the apparent seismic velocity variations introduced by changing noise source locations.

3. Results

The relative velocity variations averaged for one sensor are shown in Figure 3 along with the temporal distribution of the aftershocks. A 4 h smoothing window has been applied to time-dependent velocity variations. The velocity variations for additional sensors are given in the supporting information. The aftershocks occur minutes to hours after the blast (see Figure 3, bottom). This is much later than the arrival of the direct seismic waves, which indicates that the microseismic events are not directly triggered by the passing dynamic strain wave. The spatial clustering and delayed timing of the aftershocks indicate that they were either triggered by the changed static stress or by another mechanism.

Three remarkable features are visible in the relative velocity variation curve. First, an immediate decrease of roughly 0.025% is visible at the time of the blast. The velocity drop is followed by a slow relaxation that takes roughly 5 days. For large earthquakes in a crustal setting, the relaxation can take years [*Richter et al.*, 2014]. Finally, after 5 days the velocity has converged to a new baseline value 0.025% higher than before the blast. The immediate velocity decrease and subsequent relaxation were observed at all sensors within a 200 m radius of the blast.

The mechanism by which seismic velocities decrease in response to dynamic stress perturbations is often described as related to damage, that is, the opening of cracks or motions at the grain boundaries. Since a seismic velocity decrease is observed at all sensors close to the blast, we attribute the immediate velocity drop to damage and plastic deformation induced by the strong shaking of the production blast, whereas the subsequent relaxation is interpreted as the closing of the newly opened cracks and fractures by the confining static stress. The relaxation time was roughly similar for all sensor locations and exhibited no detectable spatial variations (see supporting information). The seismic activity rate returns to normal levels roughly 2 days after the blast, which is significantly faster than the seismic velocity changes.

Arguably the most interesting feature of the velocity variations in Figure 3 is that the seismic velocity ultimately increases in response to the blast for this sensor. This result might seem unusual, since it is expected that the seismic velocity will decrease in response to the weakening of the medium by the blast. For some other sensor locations, we do see a permanent decrease in the seismic velocity after relaxation (see supporting information). In our opinion, the only physical mechanism for an increase of the seismic velocities in this scenario could be an increase in elastic static stress due to the removal of a portion of solid rock by the blast. Such modifications to excavations cause the virgin stresses to further redistribute, producing zones of increased stress as well as zones of decreased stress. For example, if the virgin principal stress is vertical (i.e., lithostatic pressure is dominating), then removal of a thin horizontal slot will increase the volumetric stress at the abutments but decrease volumetric stress above and below the slot.

To estimate the 3-D elastic stress changes due to the blast, we constructed and solved an elastic static stress model. This entails creating a 3-D model with the mined-out regions enclosed by free surfaces and surrounded by homogeneous isotropic rock and using the displacement discontinuity boundary-element method [*Jager and Ryder*, 2002]. In short, this method estimates the value of the stress at each element in our model as the sum of the Kelvin solutions for the stress induced at this element by the virgin stress acting individually on each of the other elements in our model. This process is repeated after a 20 m^3 piece of rock is removed in the location where the blast was detonated, and the difference between the two model solutions represents the modeled static stress change. For a discussion on the effects of changes in tunnel geometry on changes in local stresses we refer the reader to *Jager and Ryder* [2002]. The virgin stress used in the model was measured by Commonwealth Scientific and Industrial Research Organisation cell overcoring measurements, and measured values of the Young's modulus and Poisson's ratio were used [*Boliden*, 2014].

To approximate the values of the velocity change between sensors, we used a 3-D triangulation-based linear interpolation method. To visualize the velocity changes, isosurfaces of the interpolated values were created. Even though it is possible to create high-resolution 3-D images of the modeled elastic static stress changes, we chose to only calculate the elastic static stress changes in the vicinity of each seismic sensor and use the same 3-D interpolation and visualization method used to visualize the velocity changes. This was done in order to minimize the influence of the interpolation method on our final interpretations. The average of all elements within 10 m of each sensor was used as the value of the modeled stress change at this sensor.

Figure 4 shows the locations of the blast and aftershocks along with immediate changes of the seismic velocity (a), the permanent changes of the seismic velocity (b), and the changes in the modeled elastic static stress (c).

The immediate changes of the seismic velocity (Figure 4a) show the decrease in seismic velocity experienced at all sensor locations due to the damage from the dynamic strain wave from the blast.

The permanent change in seismic velocity and the modeled change in volumetric stress $\frac{1}{3}(\sigma_{11} + \sigma_{22} + \sigma_{33})$ are generally in agreement for most locations—there is an increase in modeled volumetric stress to the north-east of the blast and a decrease to the south-west (Figures 4b and 4c). A comparison of the relative velocity change to the modeled stress change indicates a velocity-stress sensitivity of the order of 10^{-8}/Pa, which compares well with values reported in the literature (see table in *Yamamura et al.* [2003]). The similar spatial distribution, along with the plausible value for the velocity-stress sensitivity, indicates that the change in baseline of the seismic velocity could be a good proxy for the change in elastic static volumetric stress. Alternative explanations for the permanent changes in the seismic velocity could include pore fluid migration and pore pressure changes due to drainage after blasting and excavation.

Although the comparison between the two independent methods is qualitatively convincing, there are a few areas where the methods are not in complete agreement. The difference is especially clear in the area where the aftershocks are clustered (directly to the south of the blast in Figure 4). The presence of fractured zones, as indicated by the spatial clustering of the aftershocks, could explain the discrepancy between the modeled stress change and the observed velocity changes. In other words, the homogeneous static stress model could be too simple to accurately represent the complex rock mass in these zones.

The majority of the aftershocks are clustered in an area where we see an immediate decrease in the seismic velocity and also a change in modeled elastic static stress. However, the aftershocks are not necessarily

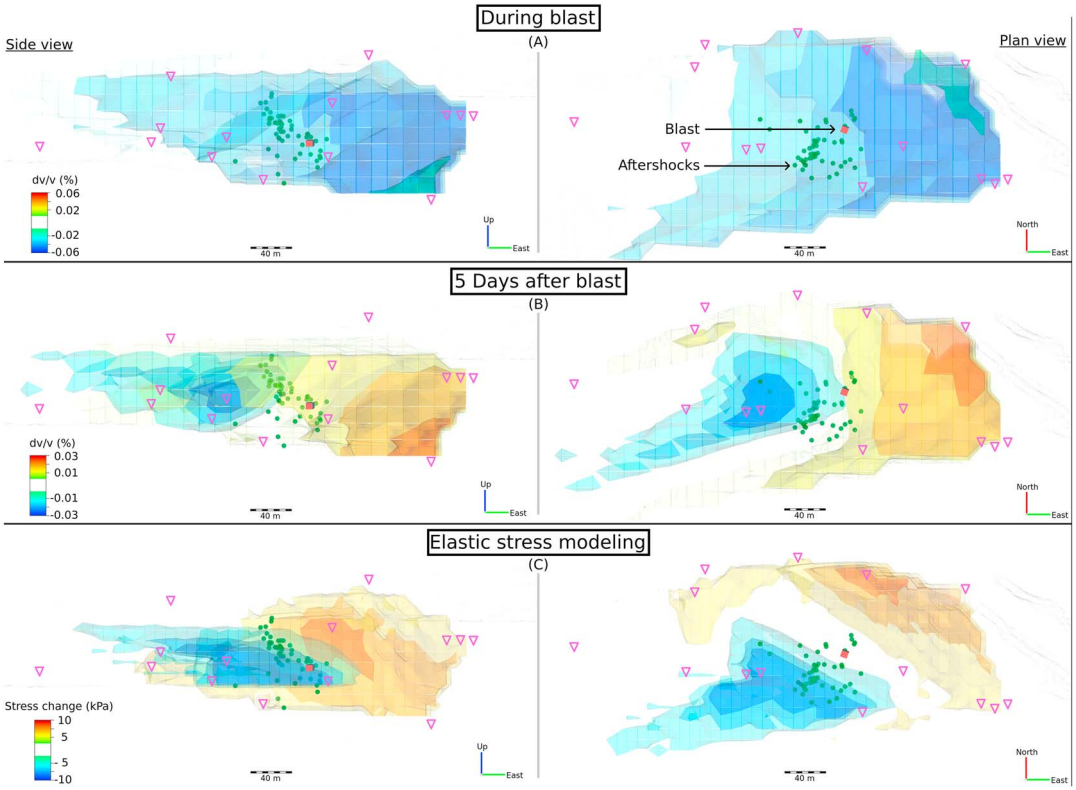

Figure 4. Comparison of isosurfaces of the immediate change in the seismic velocity, the permanent change in the seismic velocity, and the modeled volumetric stress change. The permanent change in the seismic velocity (5 days after blast) and the modeled static stress change are qualitatively in agreement for most locations.

located in areas where we see the largest change in either of these quantities. Instead, the aftershocks appear to be clustered in the vicinity of a known fault [*Boliden*, 2014]. This could indicate that the fault that was activated by the changes in elastic static stress resulting from the blast. Alternatively, the location of the cluster of aftershocks could indicate that this area was highly stressed before the deformation and more susceptible to induced fracturing. Both these observations are consistent with previous results obtained in a mine environment [*Castellanos and Van der Baan*, 2015].

4. Conclusions

An experiment was performed in which a blast was detonated in a tunnel in an underground mine, while seismic velocity variations were accurately (0.01%) measured with ambient seismic noise correlations. Additionally, aftershock activity was examined, and the influence of the removal of a portion of solid rock was estimated with elastic static stress numerical modeling. The majority of the aftershocks were delayed with respect to the passing of the dynamic waves from the blast, while the locations of the aftershocks appeared clustered and not homogeneously spread around the blast location.

A significant velocity drop is visible during the time of the blast, which is interpreted as a consequence of damage and plastic deformation. These nonelastic effects are healed by the confining stresses over a period of 5 days until the seismic velocity converges to a new baseline level. The instantaneous weakening and gradual healing observed from the velocity variations are qualitatively similar to results reported in laboratory studies. The change in the baseline level of the seismic velocity before and after the blast indicates a change in the static stress that is comparable to the results of elastic static stress modeling. The differences between the elastic model predictions and the seismic velocity variations could be due to zones of fractured rock, suggested by the spatial clustering of the aftershocks, that are not represented by the simple homogeneous isotropic elastic model.

Acknowledgments
We would like to thank Boliden's Garpenberg mine in Sweden for giving permission to use the mine plans and data; the IMS research patrons for funding the project; P. Johnson for the useful discussions; G. Basson for the help with the static stress modeling; and O. Goldbach, T. Goebel, M. Wysession, and two anonymous reviewers for their suggestions on improving the manuscript. The work of N. Shapiro was supported by the Russian Science Foundation (grant 14-47-00002).

References

Amos, C. B., P. Audet, W. C. Hammond, R. Bürgmann, I. A. Johanson, and G. Blewitt (2014), Uplift and seismicity driven by groundwater depletion in central California, *Nature*, *509*(7501), 483–486.

Bakun, W. H., and A. G. Lindh (1985), The Parkfield, California, earthquake prediction experiment, *Science*, *229*(4714), 619–624.

Boliden (2014), Laboratory measurements on core samples at Garpenberg, Internal communications.

Bouchon, M., H. Karabulut, M. Aktar, S. Özalaybey, J. Schmittbuhl, and M.-P. Bouin (2011), Extended nucleation of the 1999 M_w 7.6 Izmit earthquake, *Science*, *331*(6019), 877–880.

Brenguier, F., M. Campillo, C. Hadziioannou, N. Shapiro, R. Nadeau, and E. Larose (2008a), Postseismic relaxation along the San Andreas fault at Parkfield from continuous seismological observations, *Science*, *321*, 1478–1481.

Brenguier, F., N. Shapiro, M. Campillo, V. Ferrazzini, Z. Duputel, O. Coutant, and A. Nercessian (2008b), Towards forecasting volcanic eruptions using seismic noise, *Nat. Geosci.*, *321*, 126–130.

Brenguier, F., M. Campillo, T. Takeda, Y. Aoki, N. Shapiro, X. Briand, K. Emoto, and H. Miyake (2014), Mapping pressurized volcanic fluids from induced crustal seismic velocity drops, *Science*, *345*(6192), 80–82.

Campillo, M. (2006), Phase and correlation in random seismic fields and the reconstruction of the green function, *Pure Appl. Geophys.*, *163*, 475–502.

Castellanos, F., and M. Van der Baan (2015), Dynamic triggering of microseismicity in a mine setting, *Geophys. J. Int.*, *202*(2), 728–737.

Cheng, X., F. Niu, and B. Wang (2010), Coseismic velocity change in the rupture zone of the 2008 M_w 7.9 Wenchuan earthquake observed from ambient seismic noise, *Bull. Seismol. Soc. Am.*, *100*(5B), 2539–2550.

Clarke, D., L. Zaccarelli, N. Shapiro, and F. Brenguier (2011), Assessment of resolution and accuracy of the moving window cross spectral technique for monitoring crustal temporal variations using ambient seismic noise, *Geophys. J. Int.*, *1365*, 867–882.

Fazio, T. D., L. Aki, and K. Alba (1973), Solid earth tide and observed change in the in situ seismic velocity, *J. Geophys. Res.*, *78*, 1319–1322.

Froment, B., M. Campillo, P. Roux, P. Gouédard, A. Verdel, and R. L. Weaver (2010), Estimation of the effect of nonisotropically distributed energy on the apparent arrival time in correlations, *Geophysics*, *75*(5), SA85–SA93.

Gomberg, J., P. Reasenberg, P. Bodin, and R. Harris (2001), Earthquake triggering by seismic waves following the Landers and Hector Mine earthquakes, *Nature*, *411*(6836), 462–466.

Gomberg, J., P. Bodin, and P. A. Reasenberg (2003), Observing earthquakes triggered in the near field by dynamic deformations, *Bull. Seismol. Soc. Am.*, *93*(1), 118–138.

Gomberg, J., P. Bodin, K. Larson, and H. Dragert (2004), Earthquake nucleation by transient deformations caused by the M=7.9 Denali, Alaska, earthquake, *Nature*, *427*(6975), 621–624.

Gonzalez-Huizar, H., and A. A. Velasco (2011), Dynamic triggering: Stress modeling and a case study, *J. Geophys. Res.*, *116*, B02304, doi:10.1029/2009JB007000.

Hill, D., et al. (1993), Seismicity remotely triggered by the magnitude 7.3 Landers, California, earthquake, *Science*, *260*(5114), 1617–1623.

Hillers, G., S. Husen, A. Obermann, T. Planes, M. Campillo, and E. Larose (2014), The resolution of reservoir dynamics with noise based technologies: A case study from the 2006 Basel injection experiment, in *EGU General Assembly Conference Abstracts*, vol. 16, 7802 pp.

Jager, A., and J. Ryder (2002), *A Textbook on Rock Mechanics for Tabular Hard Rock Mines*, Safety in Mines Research Advisory Committee (SIMRAC), Johannesburg.

Johnson, P. A., and X. Jia (2005), Nonlinear dynamics, granular media and dynamic earthquake triggering, *Nature*, *437*(7060), 871–874.

Johnson, C. W., R. Burgmann, and F. F. Pollitz (2015), Rare dynamic triggering of remote $M > 5.5$ earthquakes from global catalog analysis, *J. Geophys. Res. Solid Earth*, *120*, 1748–1761, doi:10.1002/2014JB011788.

Leary, P., P. Malin, R. Phinney, T. Brocher, and R. Voncolln (1979), Systematic monitoring of millisecond travel time variations near Palmdale, California, *J. Geophys. Res.*, *84*(B2), 659–666.

Lockner, D., J. Walsh, and J. Byerlee (1977), Changes in seismic velocity and attenuation during deformation of granite, *J. Geophys. Res.*, *82*(33), 5374–5378.

Mainsant, G., E. Larose, C. Bronnimann, D. Jongmans, C. Michoud, and M. Jaboyedoff (2012), Ambient seismic noise monitoring of a clay landslide: Toward failure prediction, *J. Geophys. Res.*, *117*, F01030, doi:10.1029/2011JF002159.

Mantovani, E., M. Viti, D. Babbucci, D. Albarello, N. Cenni, and A. Vannucchi (2010), Long-term earthquake triggering in the Southern and Northern Apennines, *J. Seismolog.*, *14*(1), 53–65.

Niu, F., P. Silver, T. Daley, X. Cheng, and E. Majer (2008), Preseismic velocity changes observed from active source monitoring at the Parkfield SAFOD drill site, *Nature*, *454*, 204–208.

Nur, A. (1971), Effects of stress on velocity anisotropy in rocks with cracks, *J. Geophys. Res.*, *76*(8), 2022–2034.

O'Connell, R. J., and B. Budiansky (1974), Seismic velocities in dry and saturated cracked solids, *J. Geophys. Res.*, *79*(35), 5412–5426.

Olivier, G., F. Brenguier, M. Campillo, R. Lynch, and P. Roux (2015), Body-wave reconstruction from ambient seismic noise correlations in an underground mine, *Geophysics*, *80*(3), KS11–KS25.

Poupinet, G., W. L. Ellsworth, and J. Frechet (1984), Monitoring velocity variations in the crust using earthquake doublets: An application to the Calaveras Fault, California, *J. Geophys. Res.*, *89*(B7), 5719–5731, doi:10.1029/JB089iB07p05719.

Reasonberg, P., and K. Aki (1974), A precise, continuous measurement of seismic velocity for monitoring in situ stress, *J. Geophys. Res.*, *79*, 399–406.

Richter, T., C. Sens-Schönfelder, R. Kind, and G. Asch (2014), Comprehensive observation and modeling of earthquake and temperature-related seismic velocity changes in northern Chile with passive image interferometry, *J. Geophys. Res. Solid Earth*, *119*, 4747–4765, doi:10.1002/2013JB010695.

Roux, P., and W. Kuperman (2004), Extracting coherent wavefronts from accoustic ambient noise in the ocean, *J. Acoust. Soc. Am.*, *116*, 1995–2003.

Sabra, K., P. Roux, and W. Kuperman (2005), Emergence rate of the time-domain Green's function from the ambient noise cross-correlation function, *J. Acoust. Soc. Am.*, *118*, 3524–3531.

Scholz, C. H. (2002), *The Mechanics of Earthquakes and Faulting*, Cambridge Univ. Press, Cambridge.

Sens-Schönfelder, C., and U. Wegler (2006), Passive image interferometry and seasonal variations of seismic velocities at Merapi Volcano, Indonesia, *Geophys. Res. Lett.*, *33*, L21302, doi:10.1029/2006GL027797.

Shapiro, N. M., and M. Campillo (2004), Emergence of broadband Rayleigh waves from correlations of the ambient seismic noise, *Geophys. Res. Lett.*, *31*, L07614, doi:10.1029/2004GL019491.

Shapiro, S., R. Patzig, E. Rothert, and J. Rindschwentner (2003), Triggering of seismicity by pore-pressure perturbations: Permeability-related signatures of the phenomenon, *Pure Appl. Geophys.*, *160*(5–6), 1051–1066.

Stein, R. S. (1999), The role of stress transfer in earthquake occurrence, *Nature*, *402*(6762), 605–609.

Tape, C., M. West, V. Silwal, and N. Ruppert (2013), Earthquake nucleation and triggering on an optimally oriented fault, *Earth Planet. Sci. Lett.*, *363*, 231–241.

Vallejos, J., and S. McKinnon (2010), Omori's law applied to mining-induced seismicity and re-entry protocol development, *Pure Appl. Geophys.*, *167*(1–2), 91–106, doi:10.1007/s00024-009-0010-7.

Yamamura, K., O. Sano, H. Utada, Y. Takei, S. Nakao, and Y. Fukao (2003), Long-term observation of in situ seismic velocity and attenuation, *J. Geophys. Res.*, *108*(B6), 2317, doi:10.1029/2002JB002005.